

Layered $\text{CrGe}_{1-x}\text{Se}_{3+y}$ with Cr Kagome Lattice and Antiferromagnetic Ordering

Jeremy G. Philbrick¹, Chaoguo Wang², Xin Gui², Tai Kong^{1,3}*

¹Department of Physics, The University of Arizona, Tucson, Arizona 85721 USA

²Department of Chemistry, University of Pittsburgh, Pittsburgh, Pennsylvania 15260, USA

³Department of Chemistry and Biochemistry, The University of Arizona, Tucson, Arizona 85721 USA

KEYWORDS layered structure, magnetic ordering, Kagome.

ABSTRACT We report the synthesis and properties of a new layered material, $\text{CrGe}_{1-x}\text{Se}_{3+y}$. The crystal structure was determined by using single crystal x-ray diffraction and transmission electron microscopy. $\text{CrGe}_{1-x}\text{Se}_{3+y}$ crystallizes with a space group $R-3m$, featuring a double Kagome layer of chromium atoms, sandwiched between disordered Ge-Se layers. This compound displays antiferromagnetic order below 50 K, unlike the ferromagnetic behavior in CrGeTe_3 . Chromium displays an effective moment of $\sim 3.9 \mu_B/\text{Cr}$, consistent with Cr^{3+} oxidation. The presence of this phase limits the possibility of a ferromagnetic CrGeSe_3 analogous to CrGeTe_3 .

Introduction

Low-dimensional materials are a fruitful area of research for the discovery of novel phenomena. Although the ideal case of an isotropic two-dimensional (2D) crystal of infinite size is proven to lack any spontaneous long-range ordering according to the Mermin-Wagner theorem [1], efforts to characterize and utilize 2D magnetism have been fruitful in thin films and materials with a strong magnetic anisotropy [2]. Among van der Waals (vdW) materials, the compound CrGeTe_3 was theoretically predicted to be a 2D ferromagnetic semiconductor at monolayer limit using density functional theory (DFT) [3]. This analysis found that second and third nearest neighbors in the chromium honeycomb sublattice play an important role in the formation of a ferromagnetic state. This result was experimentally verified in 2017, with the magneto-optic Kerr effect being observed in bilayer CrGeTe_3 below ~ 45 K [4], indicating the presence of long-range ferromagnetic order. 2D ferromagnetism in vdW materials are mainly studied in three structural families: CrGeTe_3 , CrI_3 , and Fe_3GeTe_2 . CrI_3 , identified at the same time with CrGeTe_3 in 2015, also has a honeycomb Cr sub-lattice, with a Curie temperature of 61 K [5]. Fe_3GeTe_2 was discovered to possess itinerant ferromagnetism in a monolayer in 2018, with a Curie temperature of 120 K [6].

Chemical substitutions in these three compounds can expand the available 2D ferromagnetic material pool. For the CrGeTe_3 family, replacing Ge with Si produced another compound ferromagnetic at ~ 33 K [7]. For CrI_3 , variation in the chalcogen site, e.g. in CrBr_3 [8], or the transition metal site, e.g. in VI_3 [9], retains ferromagnetic ordering. In Fe_3GeTe_2 , chemical tunability in the Fe site led to the discovery of the more Fe rich series, e.g. Fe_5GeTe_2 [10], which exhibits ferromagnetism around room temperature. A recent study of Fe_3GaTe_2 also saw evidence of a ferromagnetic transition around 200 K in a 1 nm thick flake [11]. Given the chemical

similarity between tellurium and selenium, it is of great interest to explore the chemical stability of known Te-based vdW ferromagnets in their Se version. Theoretical studies indicate that compounds such as CrGeSe_3 , if crystalized in the same structure as CrGeTe_3 , would also be a 2D ferromagnetic semiconductor [12] [13] [14] [15]. Selenium-based ternary phases that chemically look similar to CrGeTe_3 are rare. On the experimental side, the existence of a Cr-Ge-Se ternary phase ($\text{Cr}_3\text{Ge}_4\text{Se}_{12}$) was suggested without a clear structural description [16]. There was a report on $\text{Ga}_6\text{Cr}_5\text{Se}_{16}$, which exhibits an alternating CrSe_6 and GaSe_4 layers [17]. A Cr-Si-Se ternary was reported to crystallize in FePSe_3 -type without further information on its magnetic properties [18]. Here we detail the process of attempting to experimentally synthesize CrGeSe_3 and the resulting production of a new layered material $\text{CrGe}_{1-x}\text{Se}_{3+y}$ instead. This result expands the knowledge of chemical stability around well-known 2D magnetic material systems.

Experimental Section

Crystals of $\text{CrGe}_{1-x}\text{Se}_{3+y}$ were produced out of a germanium-selenium high temperature solution. Starting materials, Cr (Alfa Aesar, 99.94%), Ge (ThermoScientific, 99.999%), and Se (ThermoScientific, 99.999%) were combined in an evacuated silica ampule in an atomic ratio of Cr:Ge:Se = 1:32:66, with quartz wool at the top end of the tube. The packed materials were sealed under vacuum and heated to 1073 K, cooled at 1 degree per hour to 1013 K, at which point the flux solidified. To liberate the crystals, the tube was then heated up to 1023 K and inverted once the flux was molten. The roughly one-third germanium, two-thirds selenium mixture present in the ampule begins to form GeSe_2 very near 1013 K [19], so this last increase in temperature proved necessary to ensure the flux remains molten while it drips away. A centrifuge can also be used at this stage to help remove the flux, but the small temperature range available prevents this from always being effective. The crystal synthesis of $\text{CrGe}_{1-x}\text{Se}_{3+y}$ is reminiscent of the synthesis of

MnBi_2Te_4 , where a narrow formation window and careful temperature control are needed to successfully obtain the target phase [20] [21]. This procedure resulted in a collection of small, plate-like, generally hexagonal crystals of dark color on the order of 1 mm in diameter. The visible transparent color indicates that the material is a semiconductor but several attempts to add contacts to a crystal using silver paint or indium for a resistance measurement were not successful. A typical crystal imaged with a scanning electron microscope (SEM) is shown in Figure 1b.

Single-crystal X-ray diffraction (SXRD) was conducted to measure the crystal structure and chemical composition. More than five crystals from two batches were tested for consistency. The Bruker D8 QUEST ECO diffractometer equipped with APEX5 software and Mo radiation ($\lambda_{\text{K}\alpha} = 0.71073 \text{ \AA}$) was adapted for single crystal measurements at room temperature ($\sim 296 \text{ K}$). The crystals were immersed in glycerol, then picked up and mounted on a Kapton loop. The single-crystal data acquisition was determined using the Bruker SMART software, and corrections for Lorentz and polarization effects were included. The numerical absorption correction based on crystal-face-indexing was performed by XPREP. The direct method and full-matrix least-squares on F^2 procedure within the SHELXTL package were applied to solve the crystal structure [22] [23]. Powder X-ray diffraction (PXRD) was conducted on powdered single crystals, using a Bruker D8 Discover diffractometer with a microfocus and $\text{Cu K}\alpha$ radiation ($\lambda = 1.54 \text{ \AA}$). PXRD data were analyzed using GSAS and the Le Bail method [24] [25].

X-ray photoelectron spectroscopy (XPS) measurements were conducted using a Kratos Axis 165 Ultra photoelectron spectrometer. Samples were mounted on Kratos sample pucks using carbon tape and loaded into the spectrometer fast entry backfilled with Ar gas. During these measurements, base pressure remained near or below 10^{-8} hPa . Monochromatic Al $\text{K}\alpha$ X-ray excitation was used at 300 W. All survey spectra were measured at a pass energy of 160 eV and

all elemental regions were measured at a pass energy of 20 eV and 160 eV. Charge correction was done due to some differential charging of the surface. The C1s peak was corrected to 284.8 eV. Background correction was done using either a linear or Shirley (integral) model depending on the background outside the region of interest. Quantification was done using the background subtracted areas and the Kratos Relative Sensitivity Factors found in the Kratos Vision2 processing software. The resulting data were fit using a GL30 (30% Lorentzian) model for each of the peaks.

Electron-transparent slices of the crystal (approximately 100 nm thick) were produced at the University of Arizona Lunar and Planetary Lab (LPL) Kuiper Materials Imaging and Characterization Facility (KMICF) using the FEI Helios Nanolab 660 focused ion beam scanning electron microscope (FIB-SEM) and welded to a standard Omniprobe 3-post copper lift-out grid. These slices were transferred to the facility's HF5000 Hitachi transmission electron microscope (TEM) for further measurement. Crystal structure was directly observed using the TEM operated at 200 kV, and quantitative and qualitative measurement of the elemental composition was done using energy dispersive X-ray spectroscopy (EDS). The utilized TEM is equipped with spherical aberration correction, bright field (BF), dark field (DF), and secondary electron (SE) imaging detectors, and an Oxford Instruments large solid angle (2.0 sr) X-max N 100 TLE side-entry energy dispersive x-ray spectrometer with 100 mm² windowless silicon drift detectors.

As the individual mass of each crystal was only about 0.1 mg, multiple crystals were measured together to improve the accuracy of magnetization measurements. Approximately ten crystals with a combined mass of 1.4 mg were stacked and sealed together using GE varnish for the in-plane temperature-dependent (1.8-300 K) and field-dependent (0-90 kOe) magnetization measurements using the vibrating sample magnetometer (VSM) of a Quantum Design physical property measurement system (PPMS) DynaCool. Once completed, the same stack of crystals was removed

from the sample stage and reoriented for similar perpendicular-to-plane magnetization measurements in a plastic capsule. Temperature dependent heat capacity was also measured using the same PPMS, with a cluster of crystals weighing 0.8 mg placed on a standard heat capacity puck, using a 2τ relaxation method. Because of the high mass error for this small sample, the resulting data was scaled up so that it saturated at the Dulong-Petit limit expected at high-temperature as detailed below.

Results and Discussion

The crystal structure of $\text{CrGe}_{1-x}\text{Se}_{3+y}$ ($x = 0.155$ (4); $y = 0.153$ (6)) determined by SXRD is shown in Figure 1a. See the Supplemental Material for the Crystallographic Information File [26]. Chromium atoms are displayed in blue, germanium in gray, and selenium in yellow. Several distinct chromium, germanium, and selenium layers are visible: each chromium layer is sandwiched between layers of selenium, and then between selenium layers there is an alternating pattern of germanium layers and partially occupied Ge-Se layers. The partially occupied Ge-Se layers are likely to originate from stacking fault of $\text{CrGe}_{1-x}\text{Se}_{3+y}$. Note that while the disordered layers do not involve magnetic atoms, they may still affect the interlayer magnetic interaction [27] [28]. The magnetic chromium atoms are octahedrally coordinated with six selenium atoms, forming a layer via edge sharing. These octahedrons are slightly distorted, with one axis being 5.063 Å long while the other two are 5.136 Å. Within each layer, chromium atoms form a breathing Kagome lattice. Ignoring all atoms except for the chromium and looking along the c-axis (Figure 1c) clearly shows the Kagome lattice structure of the chromium atoms. Each chromium atom's nearest neighbors are all within the ab-plane, 3.550 or 3.853 Å apart depending on the bonding angle. The alternating layered structure described above results in each layer of magnetic atoms having a paired layer about 6.2 Å away. These paired layers are lined up with each

other, so that each site has another site directly above/below it in the c-axis. Beyond each layer pair, the next nearest layer is about 9.3 Å away and is not aligned in the c-axis. The appearance of double Kagome layer is not uncommon in known compounds [29]. For chromium-based Kagome materials, $\text{CrGe}_{1-x}\text{Se}_{3+y}$ may represent a rare example of a semiconducting material [29].

To confirm the SXRD refined crystal structure, TEM measurements were conducted. Detailed results are shown in Figure 2, where the TEM images are taken from in the ab-plane of the material. In Figure 2a, the refined crystal structure is partially overlayed on top of a representative TEM image, which shows good agreement structurally. Alternating bright and dark layers in an AABAA pattern can be observed in the TEM dark-field image. The bright layers have similar appearance to the Se-Cr-Se substructure within $\text{CrGe}_{1-x}\text{Se}_{3+y}$, when viewed from the b^* direction. Additionally, the brightest parts of a dark-field TEM image are likely to contain the highest concentration of the heaviest atom in the crystal, in this case selenium. Elemental composition of this material was found through EDS to be 64.7% Se, 18.2% Cr, 17.1% Ge, which is consistent with the SCXRD refinement result. An EDS line-scan (Figure 2b), conducted at an approximately 45° angle relative to the visible layers to extend the linear distance between peaks, shows high concentrations of chromium lining up with the bright layers of the material. As the scan shows germanium and selenium more evenly distributed, there is likely selenium present in the darker layers of the material, and germanium present throughout the sample. All these data are consistent with the composition and structure determined by SXRD.

The PXRD data is shown in Figure 3a. The calculated diffraction peak positions based on SXRD refinement results match well with experimentally observed data. This consistency among diffraction results and TEM images shown in Figure 2 verifies the refined crystal structure. The results in Figure 3a were obtained from the same batch of crystals used for the magnetization

measurements that will be discussed below. Figures 3(b-d) shows the XPS results. Multiple overlapping peaks are visible for Cr above 574.2 eV, corresponding to Cr 2p spectrums. Peaks at around 577 eV and 587 eV are each split into two peaks that are roughly 1 eV apart. Similar peak splitting within this energy range was attributed to Cr²⁺ and Cr³⁺ [17] [30], or simply Cr³⁺ with satellite peaks [31].

Temperature-dependent magnetic susceptibility data of CrGe_{1-x}Se_{3+y} are shown in Figure 4. There is no appreciable difference between zero-field-cooled (ZFC) and field-cooled (FC) measurements. In Figure 4, only FC data are shown for clarity. At high temperature, there is a paramagnetic region of increasing magnetization with decreasing temperature until \sim 50 K. Fitting the Curie-Weiss law:

$$\chi = \frac{c}{T - \theta_{CW}} + \chi_0 \quad (1)$$

to the high temperature portion of the curve (between 100 and 300 K) yields a Curie-Weiss temperature of 0 K and an effective moment of 3.9 μ_B /Cr with χ_0 of -0.00158 emu/mol for the ab-direction and -9 K and 3.8 μ_B /Cr with χ_0 of -0.00313 emu/mol for the c-direction. These values for effective moment are consistent with a Cr³⁺ oxidation state. The small magnetic anisotropy visible in the graph may come from the difference in the temperature-independent χ_0 value along two crystalline orientations, which may largely originate from the different sample holders used in each orientation.

At low temperature, both the ab-plane and c-axis magnetization show behaviors that are consistent with anti-ferromagnetic ordering at around 50 K. Plotting $d\chi/T/dT$ [32] (shown in Fig. 5) and defining the maximum of the peak to be the transition temperature yields a value of \sim 45 K. The

plateauing of the magnetization when the field is perpendicular to the plane is indicative of the spins being oriented in plane.

It is worth mentioning the Bereszinski-Kosterlitz-Thouless (BKT) transition, especially given that $\text{CrGe}_{1-x}\text{Se}_{3+y}$ hosts a two-dimensional Cr Kagome lattice. The predicted magnetic susceptibility of a BKT transition in a Kagome lattice [33] exhibit weaker feature than what is observed in $\text{CrGe}_{1-x}\text{Se}_{3+y}$. Given an in-plane moment, the magnetic susceptibility feature shown in Fig. 4 is close to what is expected for a noncolinear planar antiferromagnetic state [34]. More detailed magnetic structure requires future neutron experimental support.

Isothermal field-dependent magnetization of $\text{CrGe}_{1-x}\text{Se}_{3+y}$ is shown in Figure 4b. The observed field-dependence is very similar for the two measured directions, with the magnetization largely increasing linearly with field. There is a small kink at around 10 kOe for in plane magnetization that can be associated with a meta-magnetic transition.

Figure 5 shows the temperature dependent heat capacity data measured at zero magnetic field on a cluster of crystals weighing ~ 0.8 mg. A clear peak is visible at 47.5 K, corresponding to the observed peak in magnetization at approximately the same temperature. The broadness of both this peak and the peak in $d\gamma T/dT$ mentioned above may indicate two transitions occurring in a small temperature range. The expected high temperature value of heat capacity, given by the Dulong-Petit law, is $3NR$ where N is the number of atoms per formula unit and R is the gas constant. For $\text{CrGe}_{1-x}\text{Se}_{3+y}$, this value is 124.71 J/mol*K. The small mass of the sample allows for significant error in the mass measurement. To address this, the measured data were fit using the Debye model at high temperature ($T > 60$ K) with an additional multiplicative scale factor so that a Dulong-Petit limit is reached at high temperature:

$$C_D(T) = 9NR \left(\frac{T}{\theta_D}\right)^3 \int_0^{\frac{\theta_D}{T}} \frac{x^4 e^x}{(e^x - 1)^2} dx \quad (2)$$

where C_D is the Debye heat capacity, T is the temperature, $N = 5$ is the number of atoms per formula unit and Θ_D is the Debye temperature. The best fit required scaling of the measured data up by $\sim 22\%$, roughly consistent with a mass error of 0.1-0.2 mg out of a 0.8 mg sample. The normalized data and the subsequent fits are shown in Figure 5. The Debye model fitting produced a Debye temperature of 250 K. The heat capacity data can also be fit more closely using a double Debye model of the form:

$$C_L(T) = kC_{D1}(T) + (1 - k)C_{D2}(T) \quad (3)$$

where the estimated lattice heat capacity (C_L) is a sum of two Debye heat capacities (C_{D1} , C_{D2}) with a ratio between them determined by the parameter k with some value between zero and one. This results in Debye temperatures T_{D1} equaling 108 K and T_{D2} equaling 297 K, with a k -value of 0.24. This result is consistent with the expectation that heat capacity can be better modeled by introducing a Debye fit for each elemental species in the compound [35] [36]. Considering that germanium and selenium have similar atomic mass, the fitted k -value agrees with the molar ratio of chromium in $\text{CrGe}_{1-x}\text{Se}_{3+y}$. The low temperature behavior of the heat capacity is expected to follow $C_p = \gamma T + \beta T^3$, where the linear term represents the electronic contribution to heat capacity and the cubic term the phonon contribution. As the material is semiconducting, $\gamma = 0$ at low temperature as the electrons are not free to change state and absorb energy. The upper inset of Figure 5 shows the fit of this curve at values of $T^2 < 12 \text{ K}^2$, where it has a slope of $\beta = 2.85 \times 10^{-3} \text{ J/mol} \cdot \text{K}^4$ and a y-intercept of $4 \times 10^{-3} \text{ J/mol} \cdot \text{K}^2$. Assuming that the antiferromagnetic magnon contribution, which also follows T^3 behavior like phonons [37], is small [38], the Debye

temperature is estimated to be \sim 150 K with this method. This value is within the range of Debye temperatures estimated by the double Debye model described above.

The entropy associated with magnetic ordering was estimated by subtracting the phonon contribution to the heat capacity with either the single Debye fit to capture all low temperature behavior or the double Debye fit to isolate the 47.5 K peak [39] [40] [41] [42]. The single Debye fit yielded a magnetic entropy of 11.5 J/mol*K. This value matches the expected magnetic entropy for Cr³⁺. The double Debye fit matches the overall heat capacity curve better and thus suggests less magnetic contribution. The magnetic entropy associated with the peak region, using the double Debye model as phonon contribution, is estimated to be \sim 0.98 J/mol*K. This value is similar to what is observed in other magnetic layered materials [38] [43] [44].

Conclusion

We report the synthesis of a new compound in the Cr-Ge-Se system, CrGe_{1-x}Se_{3+y}. Structurally, this compound is in the *R*-3*m* space group and forms a layered structure with several resolvable layer types. The magnetic chromium sublattice consists of separated double-layer Kagome lattices, the spacing of which produces the material's quasi-2-dimensionality. As this material was produced while trying to synthesize CrGeSe₃, any attempt to produce that compound is complicated. It is possible that CrGe_{1-x}Se_{3+y} is generally more thermodynamically favored and precludes any attempt to make vdW CrGeSe₃.

Magnetically, the Curie-Weiss temperature was measured to be in the range of 0 K to -10 K and the effective moment to be about 3.9 μ_B /Cr in CrGe_{1-x}Se_{3+y}. A Néel temperature of \sim 50 K is confirmed by both magnetization and heat capacity measurements. A weak metamagnetic transition was observed for in-plane direction within the ordered state. Influence on magnetism by

low-dimensionality and Kagome lattice present in the compound requires future, more detailed neutron scattering measurements.

ACKNOWLEDGMENT

Work done at the University of Arizona is supported by the National Science Foundation under Award No. DMR-2338229. The TEM work reported herein was acquired in the Kuiper Materials Imaging and Characterization Facility, supported by NASA (grants #NNX12AL47G and #NNX15AJ22G) and NSF (grant #1531243). We thank Yao-Jen Chang for his help with the TEM measurements. All X-ray and Ultraviolet Photoelectron Spectra were collected at the Laboratory for Electron Spectroscopy and Surface Analysis (LESSA) in the Department of Chemistry and Biochemistry at the University of Arizona using a Kratos Axis 165 Ultra DLD Hybrid Ultrahigh Vacuum Photoelectron Spectrometer. The instrument was purchased with funding from the National Science Foundation and supported by the Center for Interface Science: Solar-Electric Materials (CIS:SEM), an Energy Frontier Research Center funded by the U.S. Department of Energy and Arizona Technology and Research Initiative Fund (A.R.S. §15-1648). Work done at the University of Pittsburgh is supported by the startup funding of X. G. We'd like to thank Paul Lee for helping with XPS measurements.

FIGURES

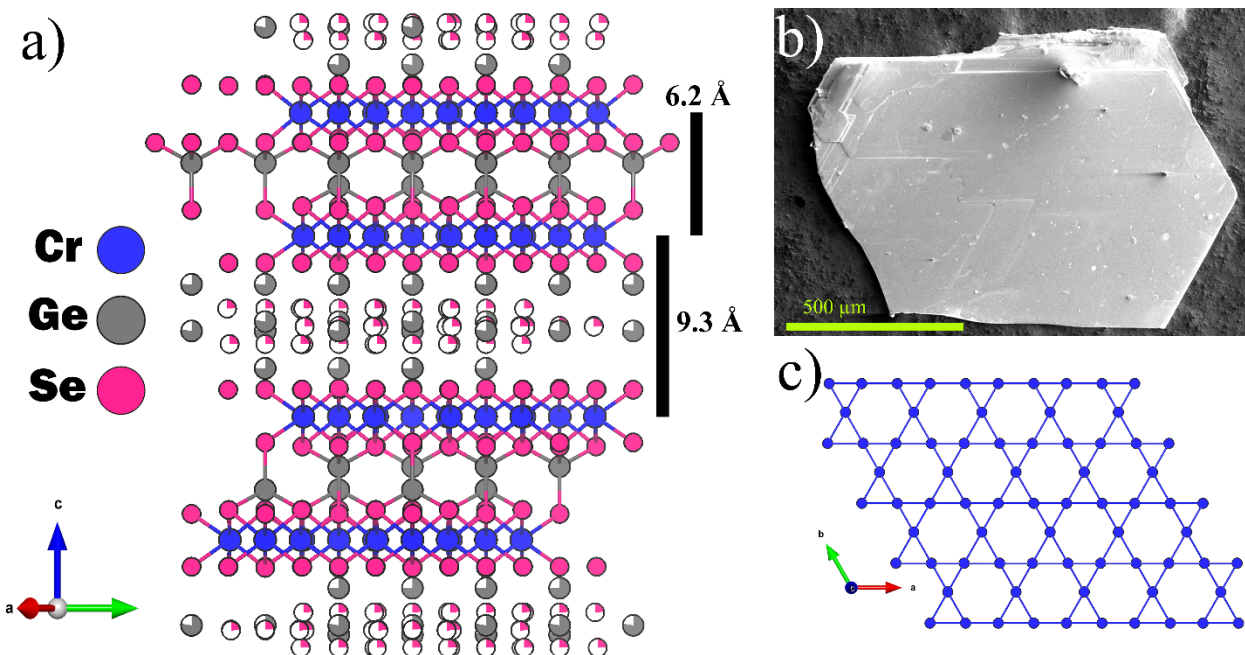


Figure 1. (a) Crystal structure viewed from b^* direction showing the layers. (b) SEM image of a representative crystal. (c) Cr sublattice forming a Kagome lattice viewed along the *c*-axis.

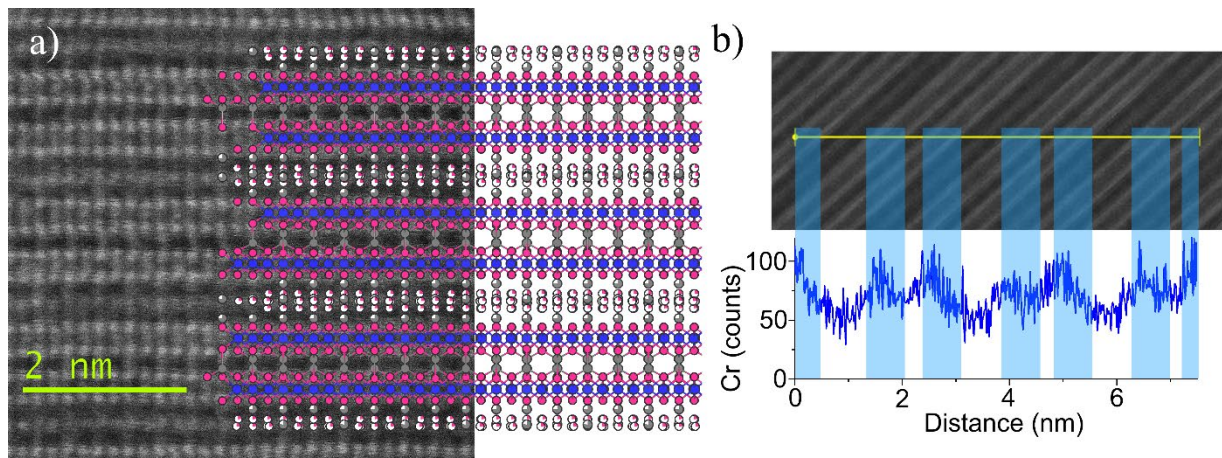


Figure 2. (a) Dark-field TEM image with overlayed crystal structure from Figure 1b. (b) TEM-EDS measurement of Cr concentration.

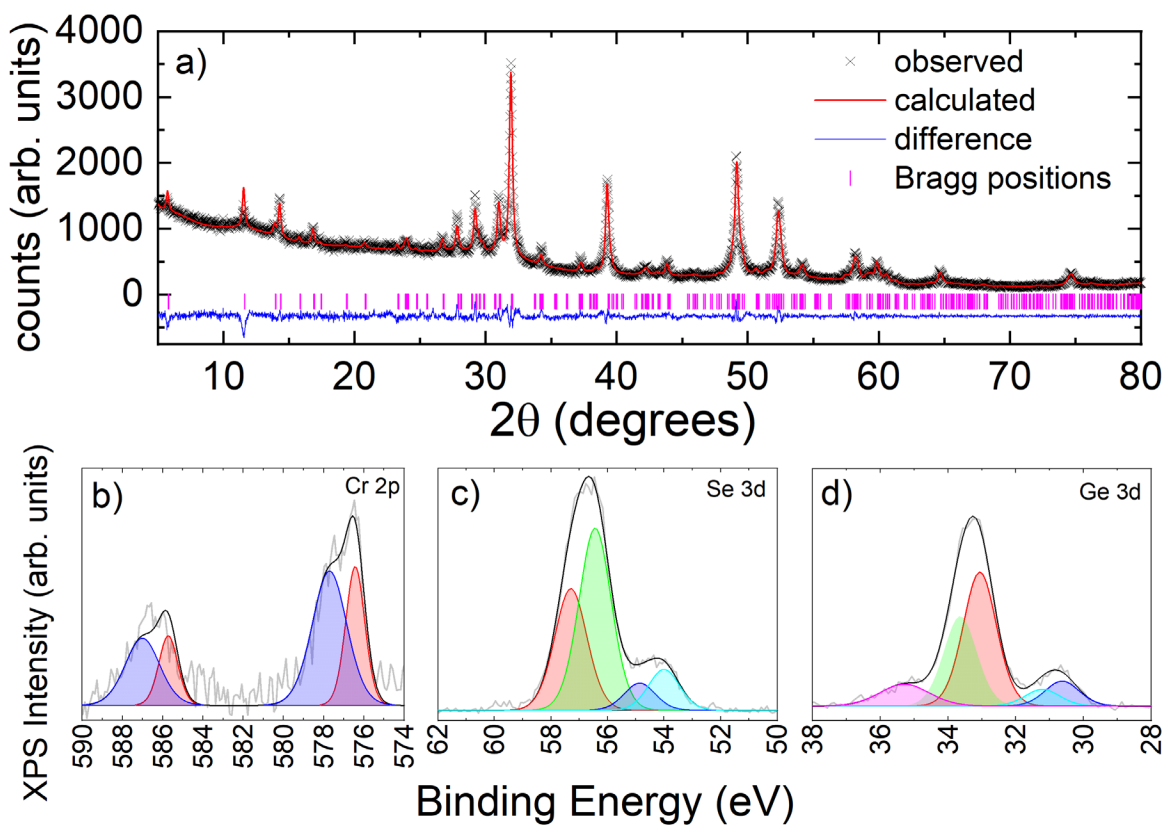


Figure 3. (a) PXRD pattern from synthesized crystals. XPS measurements of synthesized crystals at energy levels corresponding to Cr 2p (b), Se 3d (c), and Ge 3d (d).

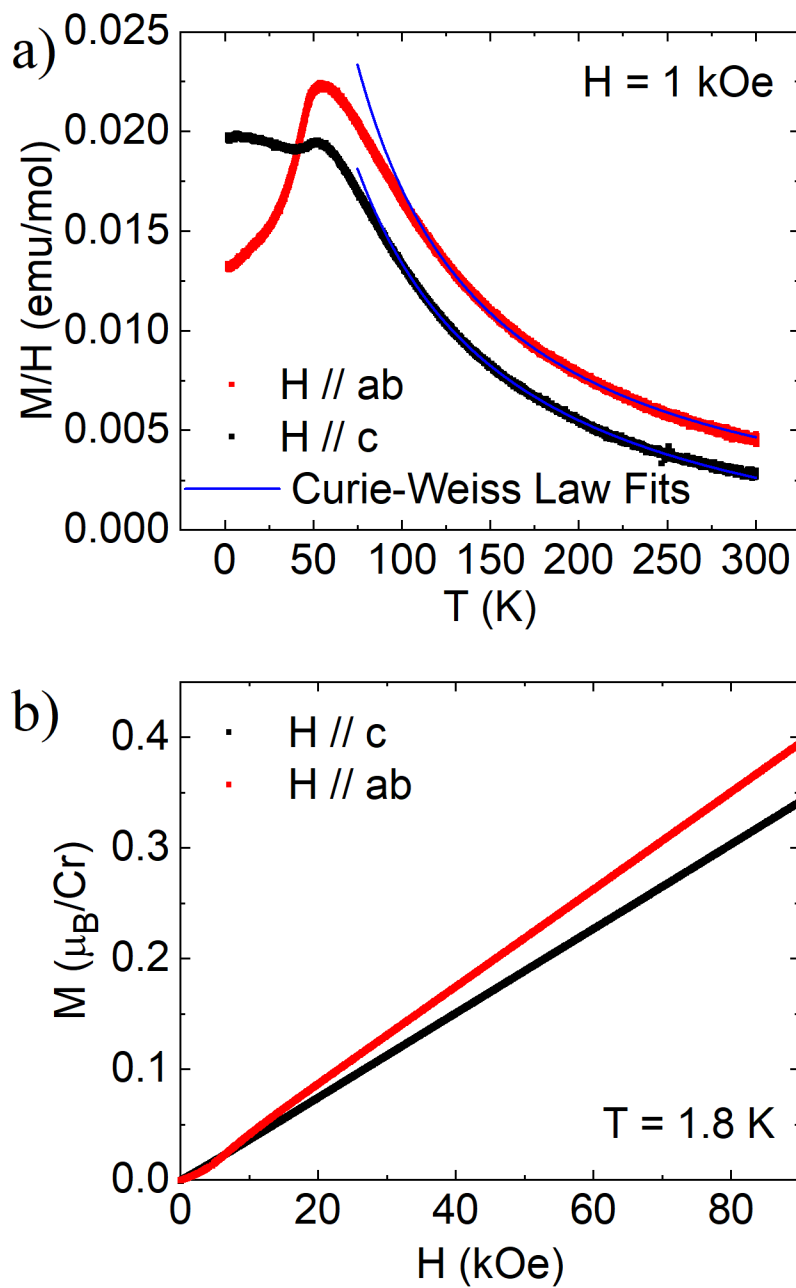


Figure 4. (a) Anisotropic temperature dependent magnetic susceptibility of $\text{CrGe}_{1-x}\text{Se}_{3+y}$. The fitting from the Curie-Weiss law is shown in blue. (b) Field-dependent magnetization per Cr atom.

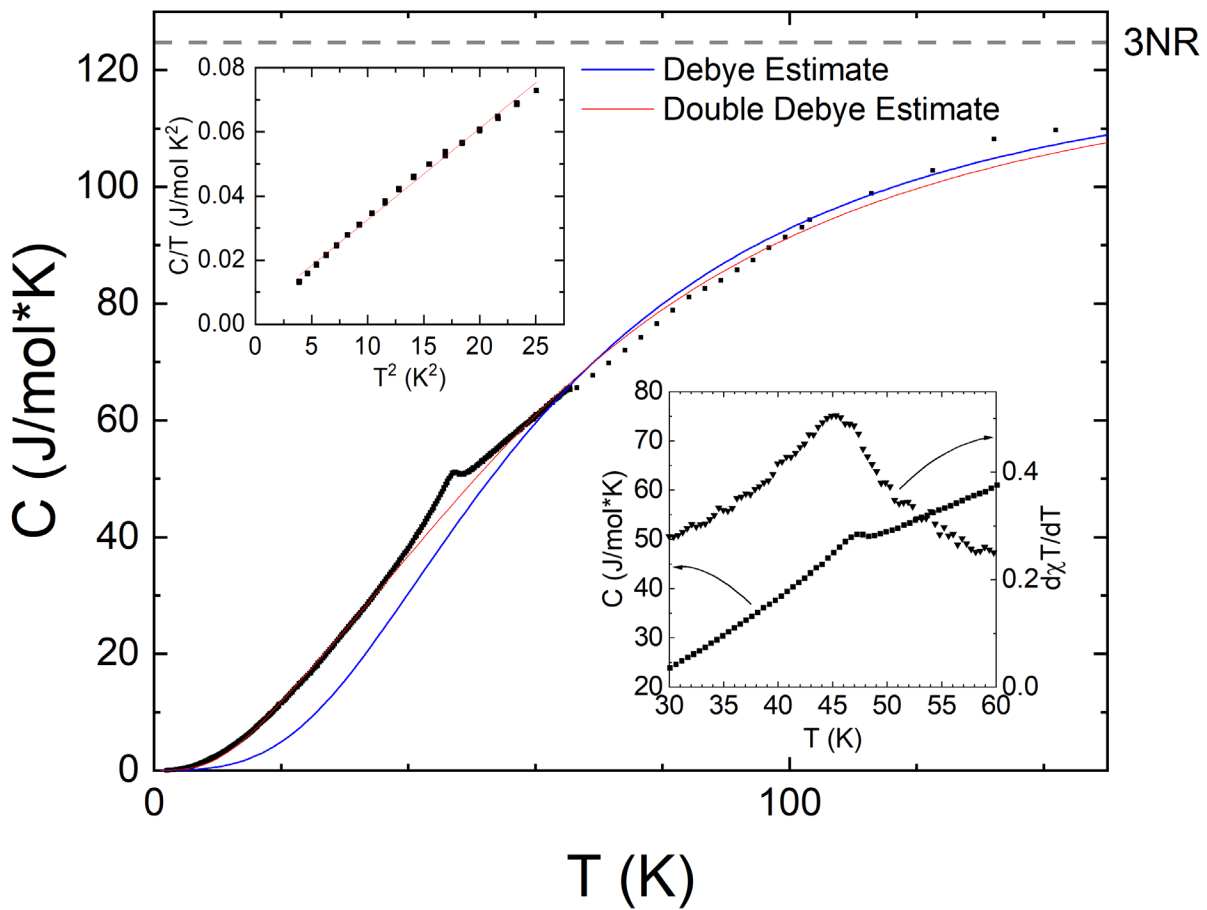


Figure 5. Zero-field, temperature-dependent specific heat of $\text{CrGe}_{1-x}\text{Se}_{3+y}$. Right inset shows a detailed view of the feature at ~ 47.5 K along with the $d\chi T/dT$ graph showing a peak at ~ 45 K. Left inset shows C/T versus T^2 at low temperatures, and a linear fit of those data.

Table 1. Single crystal structure refinement for $\text{CrGe}_{0.845(4)}\text{Se}_{3.153(6)}$ at 296(2) K.

Refined Formula	$\text{CrGe}_{0.845(4)}\text{Se}_{3.153(6)}$
Temperature (K)	296 (2)
F.W. (g/mol)	362.37
Space group; Z	$R-3m$; 18
$a(\text{\AA})$	7.4033 (3)
$c(\text{\AA})$	45.770 (3)
$V(\text{\AA}^3)$	2172.5 (2)
θ range (°)	3.208 - 34.369
No. reflections; R_{int}	21482; 0.0877
No. independent reflections	1217
No. parameters	50
R_I : ωR_2 ($I > 2\delta(I)$)	0.0391; 0.0723
Goodness of fit	1.014
Diffraction peak and hole (e ⁻ / \AA^3)	1.860; -1.175

Table 2. Atomic coordinates and equivalent isotropic displacement parameters for $\text{CrGe}_{0.845(4)}\text{Se}_{3.153(6)}$ at 296(2) K. (U_{eq} is defined as one-third of the trace of the orthogonalized U_{ij} tensor (\AA^2))

Atom	Wyck.	Occ.	x	y	z	U_{eq}
Se1	18h	1	0.49906(4)	0.50094(4)	0.06950(2)	0.0153(1)
Se2	6c	1	0	1	0.20585(2)	0.0113(2)
Se3	18h	1	0.6697(1)	0.83485(4)	0.13184(2)	0.0131(1)
Se4	18h	0.245(3)	0.1548(2)	0.8452(2)	0.99952(5)	0.0188(8)
Se5	6c	1	0	1	0.06821(2)	0.01280(2)
Se6	18h	0.242(3)	0.5058(2)	0.4942(2)	0.01944(5)	0.0166(7)
Ge1	6c	1	0	1	0.15401(2)	0.0116(2)
Ge2	6c	0.779(6)	0.3333	0.6667	0.00515(3)	0.0270(6)
Ge3	6c	0.757(5)	0.3333	0.6667	0.95393(3)	0.0149(4)
Cr1	18h	1	0.8265(1)	0.6531(1)	0.23427(2)	0.0117(2)

Table 3. Anisotropic thermal displacement parameters for $\text{CrGe}_{0.845(4)}\text{Se}_{3.153(6)}$ at 296(2) K.

Atom	U11	U22	U33	U12	U13	U23
Se1	0.0131(2)	0.0131(2)	0.0170(3)	0.0047(2)	-0.0024(1)	0.0024(1)
Se2	0.0095(3)	0.0095(3)	0.0150(4)	0.0047(1)	0	0
Se3	0.0096(2)	0.0106(2)	0.0187(3)	0.0048(1)	0.0003(2)	0.0001(1)
Se4	0.019(1)	0.019(1)	0.020(1)	0.010(1)	0.0027(4)	-0.0027(4)
Se5	0.0120(3)	0.0120(3)	0.0144(4)	0.0060(1)	0	0
Se6	0.017(1)	0.017(1)	0.015(1)	0.007(1)	-0.0013(4)	0.0013(4)
Ge1	0.0105(3)	0.0105(3)	0.0138(4)	0.0053(1)	0	0
Ge2	0.0347(7)	0.0347(7)	0.0115(7)	0.0174(4)	0	0
Ge3	0.0159(5)	0.0159(5)	0.0128(7)	0.0079(3)	0	0
Cr1	0.0098(3)	0.0086(4)	0.0164(4)	-0.0011(3)	-0.0006(1)	-0.0011(3)

REFERENCES

- [1] N. D. Mermin and H. Wagner, Absence of Ferromagnetism or Antiferromagnetism in One- or Two-Dimensional Isotropic Heisenberg Model, *Phys Rev Lett* **17**, 1133 (1966).
- [2] H. C. Siegmann, Surface and 2D Magnetism, *Journal of Physics: Condensed Matter* **4**, 8395 (1992).
- [3] N. Sivadas, M. W. Daniels, R. H. Swendsen, S. Okamoto, and D. Xiao, Magnetic ground state of semiconducting transition-metal trichalcogenide monolayers, *Phys Rev B Condens Matter Mater Phys* **91**, 235425 (2015).
- [4] C. Gong et al., Discovery of intrinsic ferromagnetism in two-dimensional van der Waals crystals, *Nature* **546**, 265 (2017).
- [5] M. A. McGuire, H. Dixit, V. R. Cooper, and B. C. Sales, Coupling of crystal structure and magnetism in the layered, ferromagnetic insulator CrI₃, *Chemistry of Materials* **27**, 612 (2015).
- [6] Z. Fei et al., Two-dimensional itinerant ferromagnetism in atomically thin Fe₃GeTe₂, *Nat Mater* **17**, 778 (2018).
- [7] T. J. Williams, A. A. Aczel, M. D. Lumsden, S. E. Nagler, M. B. Stone, J. Q. Yan, and D. Mandrus, Magnetic correlations in the quasi-two-dimensional semiconducting ferromagnet CrSiTe₃, *Phys Rev B Condens Matter Mater Phys* **92**, 144404 (2015).
- [8] Z. Zhang, J. Shang, C. Jiang, A. Rasmita, W. Gao, and T. Yu, Direct Photoluminescence Probing of Ferromagnetism in Monolayer Two-Dimensional CrBr₃, *Nano Lett* **19**, 3138 (2019).
- [9] T. Kong, K. Stolze, E. I. Timmons, J. Tao, D. Ni, S. Guo, Z. Yang, R. Prozorov, and R. J. Cava, VI 3 — a New Layered Ferromagnetic Semiconductor, *Advanced Materials* **31**, 1808074 (2019).
- [10] A. F. May, D. Ovchinnikov, Q. Zheng, R. Hermann, S. Calder, B. Huang, Z. Fei, Y. Liu, X. Xu, and M. A. McGuire, Ferromagnetism Near Room Temperature in the Cleavable van der Waals Crystal Fe 5 GeTe 2, *ACS Nano* **13**, 4436 (2019).
- [11] Z. Chen, Y. Yang, T. Ying, and J. G. Guo, High-Tc Ferromagnetic Semiconductor in Thinned 3D Ising Ferromagnetic Metal Fe₃GaTe₂, *Nano Lett* **24**, 993 (2024).
- [12] Z. Shen, X. Fan, D. Yang, Y. Gong, S. Ma, N. Guo, Y. Hu, E. Benassi, and W. Lau, First-principles study the single-layer transition metal trihalide CrXSe₃ (X = Sn, Ge, Si) as monolayer ferromagnetic semiconductor, *Journal of Physics Condensed Matter* **32**, 085801 (2020).
- [13] J. Y. You, X. J. Dong, B. Gu, and G. Su, Possible Room-Temperature Ferromagnetic Semiconductors, *Chinese Physics Letters* **40**, 067502 (2023). 20
- [14] G. Martínez-Carracedo, A. García-Fuente, L. Oroszlány, L. Szunyogh, and J. Ferrer, Tuning magnetic exchange interactions in two-dimensional magnets: The case of CrGeX₃ (X = Se, Te) and Janus Cr₂Ge₂(Se,Te)3 monolayers, *Phys Rev B* **110**, 184406 (2024).

[15] M. S. Baranova and V. R. Stempitsky, Magnetic properties of low-dimensional MAX3 (M=Cr, A=Ge, Si and X=S, Se, Te) systems, Materials Physics and Mechanics **49**, 73 (2022).

[16] K. Villars Pierre and Cenzual, editor , *Cr₃Ge₄Se₁₂ Crystal Structure: Datasheet from "PAULING FILE Multinaries Edition – 2022,"* https://materials.springer.com/isp/crystallographic/docs/sd_1921921.

[17] N. Ma et al., Phonon Symphony of Stacked Multilayers and Weak Bonds Lowers Lattice Thermal Conductivity, Advanced Materials **34**, 2202677 (2022).

[18] J. Qopalakrishnan and K. S. Nanjundaswamy, New Transition Metal Silicoselenides Possessing CdI₂-Type Structures, Mat. Res. Bull **23**, 107 (1988).

[19] A. B. Gokhale and R. Abbaschian, The Ge-Se (Germanium-Selenium) System, Bulletin of Alloy Phase Diagrams **11**, 257 (1990).

[20] J. Q. Yan, Y. H. Liu, D. S. Parker, Y. Wu, A. A. Aczel, M. Matsuda, M. A. McGuire, and B. C. Sales, A-type antiferromagnetic order in MnBi₄Te₇ and MnBi₆Te₁₀ single crystals, Phys Rev Mater **4**, 054202 (2020).

[21] Z. S. Aliev et al., Novel ternary layered manganese bismuth tellurides of the MnTe-Bi₂Te₃ system: Synthesis and crystal structure, J Alloys Compd **789**, 443 (2019).

[22] N. Walker and D. Stuart, PROMETHEUS. Program system for structure refinements, Acta Cryst. **29**, 158 (1983).

[23] G. M. Sheldrick, Crystal structure refinement with SHELXL, Acta Crystallogr C Struct Chem **71**, 3 (2015).

[24] B. H. Toby, EXPGUI, a graphical user interface for GSAS, J Appl Crystallogr **34**, 210 (2001).

[25] A. Larson and R. Von Dreele, Generalized Structure Analysis System, University of California, 1988.

[26] The Crystallographic Information File can be found at [URL]. Alternatively, CCDC 2440742 contains supplementary crystallographic data for this paper. These data can be obtained free of charge via www.ccdc.cam.ac.uk/data_request/cif, or by emailing data_request@ccdc.cam.ac.uk, or by contacting The Cambridge Crystallographic Data Centre, 12 Union Road, Cambridge CB2 1EZ, UK; fax: +44 1223 336033

[27] C. Hu, T. Qian, and N. Ni, *Recent Progress in MnBi_{2n}Te_{3n+1} Intrinsic Magnetic Topological Insulators: Crystal Growth, Magnetism and Chemical Disorder*, National Science Review.

[28] H. Iturriaga et al., Magnetic properties of intercalated quasi-2D Fe_{3-x}GeTe₂ van der Waals magnet, NPJ 2D Mater Appl **7**, 56 (2023).

[29] V. Meschke, P. Gorai, V. Stevanović, and E. S. Toberer, Search and Structural Featurization of Magnetically Frustrated Kagome Lattices, Chemistry of Materials **33**, 4373 (2021). 21

[30] Y. Wang, W. Zhao, B. Wang, Z. Song, H. Yang, F. Wang, X. Xu, and Y. Liu, Structural diversity dependent cation incorporation into magnetic Cr-Se nanocrystals, *Nanoscale* **17**, 9222 (2025).

[31] D. Zhang, C. Yi, C. Ge, W. Shu, B. Li, X. Duan, A. Pan, and X. Wang, Controlled vapor growth of 2D magnetic Cr₂Se₃ and its magnetic proximity effect in heterostructures, *Chinese Physics B* **30**, 097601 (2021).

[32] M. E. Fisher, Relation between the specific heat and susceptibility of an antiferromagnet, *Philosophical Magazine* **7**, 1731 (1962).

[33] Y. Zhao, W. Li, B. Xi, Z. Zhang, X. Yan, S. J. Ran, T. Liu, and G. Su, Kosterlitz-Thouless phase transition and re-entrance in an anisotropic three-state Potts model on the generalized kagome lattice, *Phys Rev E Stat Nonlin Soft Matter Phys* **87**, 032151 (2013).

[34] D. C. Johnston, Magnetic susceptibility of collinear and noncollinear Heisenberg antiferromagnets, *Phys Rev Lett* **109**, 077201 (2012).

[35] J. A. Hofman, A. Paskin, K. J. Tauer, and R. J. Weiss, Analysis of Ferromagnetic and Antiferromagnetic Second-Order Transitions, *Journal of Physics and Chemistry of Solids* **1**, 45 (1956).

[36] M. Bouvier, P. Lethuillier, and D. Schmitt, Specific heat in some gadolinium compounds. I. Experimental, *Phys Rev B* **43**, 137 (1991).

[37] A. Tari, *The Specific Heat of Matter at Low Temperatures* (World Scientific, 2003).

[38] Z. Shu, H. Wang, N. H. Jo, C. Jozwiak, A. Bostwick, E. Rotenberg, W. Xie, and T. Kong, Synthesis and physical properties of a new layered ferromagnet Cr_{1.21}Te₂, *Phys Rev Mater* **7**, 044406 (2023).

[39] G. T. Lin et al., Tricritical behavior of the two-dimensional intrinsically ferromagnetic semiconductor CrGeTe₃, *Phys Rev B* **95**, 245212 (2017).

[40] Q. L. Pei et al., Spin dynamics, electronic, and thermal transport properties of two-dimensional CrPS₄ single crystal, *J Appl Phys* **119**, 043902 (2016).

[41] N. V. Kazak et al., Uniaxial anisotropy and low-temperature antiferromagnetism of Mn₂BO₄ single crystal, *J Magn Magn Mater* **393**, 316 (2015).

[42] R. Sankar, I. P. Muthuselvam, K. Rajagopal, K. Ramesh Babu, G. S. Murugan, K. S. Bayikadi, K. Moovendaran, C. Ting Wu, and G. Y. Guo, Anisotropic Magnetic Properties of Nonsymmorphic Semimetallic Single Crystal NdSbTe, *Cryst Growth Des* **20**, 6585 (2020).

[43] D. C. Freitas, R. Weht, A. Sulpice, G. Remenyi, P. Strobel, F. Gay, J. Marcus, and M. Núñez-Regueiro, Ferromagnetism in layered metastable 1T-CrTe₂, *Journal of Physics Condensed Matter* **27**, 176002 (2015). 22

[44] S. Selter, G. Bastien, A. U. B. Wolter, S. Aswartham, and B. Büchner, Magnetic anisotropy and low-field magnetic phase diagram of the quasi-two-dimensional ferromagnet Cr₂Ge₂Te₆, Phys Rev B **101**, 014440 (2020).